Nuclear Inst. and Methods in Physics Research, A 1055 (2023) 168495

Contents lists available at ScienceDirect

Nuclear Inst. and Methods in Physics Research, A

journal homepage: www.elsevier.com/locate/nima

Full Length Article

The effect of ground motion on the LHC and HL-LHC beam orbit

M. Schaumann [a,*], D. Gamba [a], H. Garcia Morales [a,b], R. Corsini [a], M. Guinchard [a], L. Scislo [a,c], J. Wenninger [a]

[a] CERN, Geneva, Switzerland
[b] John Adams Institute, Oxford, United Kingdom
[c] Cracow University of Technology, Cracow, Poland

ARTICLE INFO

Keywords:
Circular colliders
Orbit stability
Ground motion
Seismology
Civil engineering
Transfer functions

ABSTRACT

The High Luminosity Large Hadron Collider (HL-LHC) will require unprecedented orbit stability at the low-beta experiments, ATLAS and CMS. Because the effect of seismic noise might become a relevant source of luminosity loss, several studies have been conducted to characterise the actual ground motion in the LHC tunnel. In preparation for the official groundbreaking of the civil engineering work for the high luminosity upgrade, that started on 15 June 2018 in parallel to LHC beam operation, seismic sensors were installed to permanently monitor the ground stability close to these experiments. Compactor work and shaft excavation were expected to induce vibrations in the accelerator magnets that would cause orbit disturbance, beam loss and potentially premature beam dumps. This paper summarises the observations made on the LHC beams and uses this data to benchmark estimates of the impact of low frequency vibrations on the closed orbit at the main interaction points and collimators. The impact of ground motion on HL-LHC operation is then estimated using the expected operational scenario and the estimated mechanical stability of the new HL-LHC triplet magnets that is based on recent measurements of mechanical magnet transfer functions.

1. Motivation

Seismic activity from natural sources (e.g. earthquakes) or cultural (i.e. human-made) origin, including civil engineering works, excite ground vibrations that can be transmitted onto the circulating beam through the accelerator elements. The main effect is the change of the beam position (orbit) all along the circumference of the accelerator due to the displacement of the quadrupoles. If the orbit changes are too large and too fast, beam losses on the collimators will lead to a beam abort. Repeated beam aborts affect the integrated luminosity performance of a collider. Smaller but frequent excitation could also affect luminosity production by the reduction of the beam overlap at the Interaction Points (IP).

The impact of ground motion is of concern for most accelerators and storage rings [1]. For the Large Hadron Collider (LHC) it was studied (e.g. in [2,3]) on the basis of the experience gained at its predecessor, the Large Lepton Positron collider (LEP), and the Super Proton Synchrotron (SPS). The expected orbit drift along a fill and from fill to fill was assessed with the main conclusion being that in quiet conditions the ground motion for frequencies above 1 Hz could be neglected, and that below 1 Hz the orbit drifts were dominated by random ground motion, which could be taken care of using a low bandwidth orbit feedback. This was confirmed by the operational experience with the LHC [4]: with only earthquakes giving a measurable short-term degradation of the machine performance. Note that earthquakes are rare events and their effect on the LHC beam depends on their magnitude and distance from the epicentre. Many such events were observed on the LHC beams, but so far no beam dump was caused.

In the beginning of 2017 CERN deployed a seismic network (see Section 4.1 and Ref. [5,6]) in view of future ground motion sensitive projects that are planned in parallel to the LHC beam operation, such as High Luminosity LHC (HL-LHC) civil engineering (CE) [7] and geothermal exploitation in the Geneva canton (Geothermie2020 [8,9]).

The HL-LHC project requires new large infrastructures and services for powering and cooling of the new inner triplet quadrupoles and RF crab-cavities around the two main interaction points IP1 and IP5, where the experiments ATLAS and CMS are located, respectively. The HL-LHC CE campaign started in April 2018 with different types of surface works, e.g. the construction of new infrastructure and buildings, before the official ground breaking on 15 June. The excavation of the shafts started mid of August 2018. The risk of vibrations up to about 100 Hz generated by CE was evaluated carefully beforehand [6,10] and seismic sensors were installed in critical locations.

In this framework it is also important to verify that the present low-frequency ground motion levels are compatible with HL-LHC operation.

* Correspondence to: DESY, Hamburg, Germany.
E-mail addresses: Michaela.Schaumann@desy.de (M. Schaumann), Davide.Gamba@cern.ch (D. Gamba), Hector.Garcia.Morales@cern.ch (H. Garcia Morales).

https://doi.org/10.1016/j.nima.2023.168495
Received 5 June 2023; Accepted 23 June 2023
Available online 28 June 2023

This includes a review of the design of the cold mass support and an evaluation of the need to upgrade the present orbit feedback.

The aim of this paper is to give an overview of the observations and understanding of ground motion effects on the LHC beams and to present the expected impact of ground motion on HL-LHC operation.

2. Theoretical background

The impact of ground motion on accelerator performance depends on the timescale and frequency of the motion under consideration. The power spectral density of ground motion decreases with $1/f$, thus the amplitudes of the spectrum decrease for higher frequencies, and it become less likely to be visible on the beam unless a strong mechanical resonance or betatron side band is excited. At low frequency up to 1 Hz and over long time scales, i.e. days or months, ground motion translates in general to misalignment of the accelerators components, requiring continuous beam orbit correction [2–4] and eventually machine re-alignment campaigns. In LHC and HL-LHC, where the revolution frequency is $f_{\text{rev}} \approx 11\,245$ Hz, and for transverse optics tune $Q \approx 0.31$, the first betatron side-band frequency is at about 3.5 kHz. Noise source at this high frequency are expected to have an impact on emittance growth, which have been studied extensively for example in [11–13]. In this work, we aim to study the low frequency range between a few Hz and up to about 100 Hz, which is the range of the available ground motion sensors used in the CERN seismic network. In this range of frequency no emittance growth is expected nor observed [11] over time scales of up to the order of a few hours, therefore this work concentrates on closed orbit perturbations.

The amplitude of the closed orbit perturbation due to ground motion is expected to be much smaller than the beam size (see below). In this regime, non-linear effects, including beam–beam, which is the main source of non-linearity in LHC, can be neglected and the LHC can be assumed to be linear. In this case, the closed orbit Δx_s and angle $\Delta x'_s$ variation at a location s due to a static kick θ_{s_0} generated at a location s_0, are given by:

$$\Delta x_s = \theta_{s_0} \sqrt{\beta_s \beta_{s_0}} \frac{\cos(\pi Q_x - 2\pi\phi_{s_0 s})}{2\sin(\pi Q_x)} \tag{1}$$

$$\Delta x'_s = \frac{\theta_{s_0}}{2\sin\pi Q_x} \sqrt{\frac{\beta_{s_0}}{\beta_s}} \sin(\pi Q_x - 2\pi\phi_{s_0 s}) - \frac{\alpha_s}{\beta_s}\Delta x_s \tag{2}$$

where $\phi_{s_0 s}$ is the phase advance (in units of 2π) from s_0 to s, Q_x the machine tune and $\beta_{s_0/s}$ are the Twiss beta-functions at s_0 and s, respectively, and α_s the Twiss alpha function at s. Note that $\phi_{s_0 s}$ must be positive and is computed as

$$\phi_{s_0 s} = \begin{cases} \phi_s - \phi_{s_0}, & \text{if } (\phi_s - \phi_{s_0}) \geq 0 \\ \phi_s - \phi_{s_0} + Q_x, & \text{otherwise.} \end{cases} \tag{3}$$

The main sources of transverse kicks due to ground motion in an accelerator are the quadrupoles. In this case, the kick induced by the displacement Δx_q of a single quadrupole (q) is

$$\theta_{s_0} = \Delta x_q (K1L)_q, \tag{4}$$

where $(K1L)_q$ is the integrated strength of the quadrupole.

Eq. (1) with Eq. (4) at the position of $s_0 = q$ normalised by the local beam size (neglecting the dispersion contribution) becomes:

$$\frac{\Delta x_s}{\sqrt{\beta_s \epsilon_N/\gamma}\Delta x_q} = \frac{\sqrt{\beta_q}(K1L)_q}{\sqrt{\epsilon_N/\gamma}} \frac{\cos(\pi Q_x - 2\pi\phi_{qs})}{2\sin(\pi Q_x)} \tag{5}$$

where ϵ_N is the normalised beam emittance and γ is the relativistic factor.

Within the assumption of a perfectly linear machine, the impact of each quadrupole misalignment can be treated independently. The contributions for each quadrupole can be summed up directly or in quadrature depending on whether the motion is correlated or uncorrelated.

The LHC is mainly made of two aperture quadrupoles with the exception of the triplets on each side of the IPs that have a single common aperture. In both cases we assume that the transverse displacement of a quadrupole affects both beams in a fully correlated way, which is taken into account in the presented results.

The instantaneous luminosity is one of the key parameters to measure the performance of a collider. Assuming equal Gaussian head-on colliding beams, it is defined as [14]:

$$\mathcal{L} = \frac{N^2 f_{\text{rev}} N_b}{4\pi\sigma_{\text{IP}}^2} W \tag{6}$$

where N_b is the number of colliding bunches, N is the number of particles per bunch, σ_{IP} is the transverse beam size at the IP (assumed to be equal for both beams and planes) and

$$W = e^{-\frac{1}{4}\left(\frac{\delta_s}{\sigma_{\text{IP}}}\right)^2} \tag{7}$$

is a reduction factor that considers the beam orbit separation δ_s of the colliding beams at the IP. Using Eq. (7) one can estimate that an instantaneous luminosity loss of 1% has to be expected for an orbit separation at the IP of $\delta_s \approx 0.2\sigma_{\text{IP}}$.

The orbit separation can be either static or vary along a given time or fill, as in the case of a ground-motion driven beam orbit oscillation. Assuming a random Gaussian beam orbit separation with rms equal to σ_s, the mean value $\langle W \rangle$ results to be:

$$\langle W \rangle = \frac{\sqrt{2}}{\sqrt{\sigma_s^2/\sigma_{\text{IP}}^2 + 2}}. \tag{8}$$

For small orbit separation, the luminosity reduction based on a static separation (Eq. (7)) and a varying separation (Eq. (8)) are comparable, if $\delta_s = \sigma_s$. For an integrated luminosity loss below 1%, the rms orbit separation stability at the IP (σ_s) must be:

$$\sigma_s < 0.2\sigma_{\text{IP}}. \tag{9}$$

This simple calculation does not consider emittance dilution effects, which could become dominant for large amplitude oscillations, especially due to the strong beam–beam effect.

Considering the orbit separation calculated in Eq. (9), Ref. [15] shows that this value lies well within the linear regime of the beam–beam force, supporting the above made linear approximation. Because ground-motion-induced orbit offsets at the IP will be much smaller than the beam size, the additional closed orbit deformation from beam–beam effects is neglected in the presented analysis.

Eq. (5) is used to compute the impact of each quadrupole displacement on the closed orbit variation at a given point in the ring, e.g. at an IP. By merging this information with Eq. (7) or Eq. (8) the impact of quadrupole displacements on luminosity can be estimated. Both aspects are covered in the following sections.

3. Optics sensitivity

The amplification factor between the source quadrupole displacement and resulting orbit offset at a given location can be calculated with Eq. (5). It is a powerful tool to study the sensitivity of the beam orbit in critical locations like at the IPs and collimators. Eq. (5) only depends on the implemented optics and some known beam parameters. For the following analysis we consider two cases:

1. The nominal LHC optics used in 2018, which was partially profiting from the Achromatic Telescopic Squeeze (ATS) concept [16] ($\beta^* = 30$ cm, 6.5 TeV, $\epsilon_N = 2$ μm) [17].
2. The HL-LHC baseline optics at the end of the fill, i.e. for fully squeezed optics ($\beta^* = 15$ cm, 7 TeV, $\epsilon_N = 2.5$ μm) [18,19].

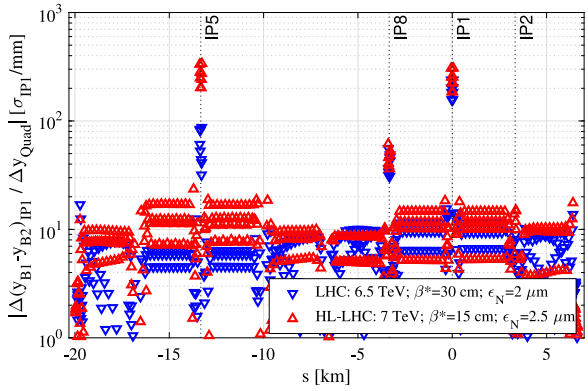

Fig. 1. Amplification factor of the IP1 vertical beam orbit separation induced by a displacement of a given quadrupole as a function of the quadrupole's location along the LHC circumference for LHC (blue) and HL-LHC (red). The location of the IPs is highlighted. All values are given in rms beam sigmas at IP1 (σ_{IP1}) per mm of quadrupole rms displacement (Δy_{Quad}).

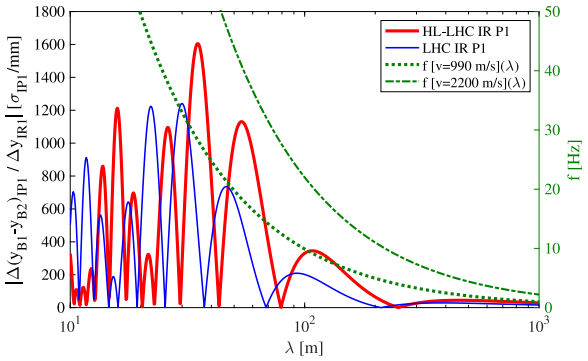

Fig. 2. Maximum vertical beam orbit separation at IP1 under the effect of a sinusoidal vibration along the whole IR1 for LHC (blue) and HL-LHC (red) as a function of the vibration wavelength. Values are given in rms beam sigmas at the IP1 (σ_{IP1}) per mm of triplet quadrupole rms displacement (Δy_{IR1}). The green curves give the wave frequency (right axis) assuming two extreme wave propagation speeds.

Table 1
Amplification factors (K_x and K_y, horizontal and vertical, respectively) between uncorrelated motion at all quadrupoles or only at IR1/5 triplets and beam separation jitter in all IPs for LHC ($\beta^* = 30$ cm; $\epsilon_N = 2$ μm; E = 6.5 TeV) and HL-LHC ($\beta^* = 15$ cm; $\epsilon_N = 2.5$ μm; E = 7 TeV). All values are given in rms beam sigmas per μm of quadrupole rms displacement.

	IP1/5		IP2		IP8	
	K_x	K_y	K_x	K_y	K_x	K_y
LHC all quads	0.8	0.6	0.3	0.4	0.4	0.5
LHC IR1/5 only	0.8	0.6	0.2	0.2	0.3	0.4
HL-LHC all quads	1.1	1.1	0.4	0.5	0.5	0.8
HL-LHC IR1/5 only	1.0	1.0	0.3	0.5	0.3	0.8

3.1. Orbit separation at the IP

Fig. 1 shows the effect of a vertical displacement at each individual quadrupole on the amplification factor, defined as the ratio between the induced vertical orbit separation of the two beams at IP1 and the generating vertical displacement of each individual quadrupole, as computed by using Eq. (5) for both LHC and HL-LHC configurations. The most sensitive quadrupoles are those of the inner triplet of the low-beta IPs (IP1 and IP5), mainly due to the extremely high beta-function, which is of the order of 7 km in the LHC and above 20 km in the HL-LHC. The non-local impact of a triplet displacement is also visible: especially for the HL-LHC, where a displacement of the IP5 triplet can induce an orbit separation in IP1 with an amplitude comparable to the one induced by a displacement of the local IP1 triplet. In the HL-LHC the impact of the arcs adjacent to IP1/5 is enhanced with respect to the LHC due to the introduction of the full Achromatic Telescopic Squeeze (ATS) optics [16],[1] but it remains well below the impact of the IP1/5 triplets. Note that this calculation evaluated at the other IPs, not shown here, gives the same qualitative result (including the enhancement around IP1/5) with slightly modified amplification amplitudes for IP2 and IP8 owing to the different beta-functions.

Assuming a fully uncorrelated and uniformly distributed ground motion along the whole accelerator, the contributions of all individual quadrupoles can be summed in quadrature, obtaining the amplification factors reported in Table 1 for both planes and all IPs.

Note that these results are dominated by the contributions of the triplets in IP1 and IP5, as can also be seen from Fig. 1 for both LHC and HL-LHC. Table 1 concludes that the HL-LHC will in general be about 50% more sensitive to magnet motion than the LHC.

Assuming to set the tolerated limit to 1% luminosity loss, the required transverse stability of the magnetic axis can be expressed as:

$$\sigma_{\text{magnet}}\ [\mu\text{m}] < \frac{0.2}{K} \tag{10}$$

where K is the relevant amplification factor from Table 1, and the 0.2 coefficient is obtained from Eq. (9).

The Interaction Region (IR), counting from the third quadrupole on the left (Q3L) to the third quadrupole on the right (Q3R), has a length of approximately 110 m and 130 m for LHC and HL-LHC, respectively. The length of one triplet is approximately 30 m and 40 m for LHC and HL-LHC, respectively. The values in Table 1 have been computed assuming that each quadrupole vibrates independently of each other. In contrast to this, Fig. 2 shows the maximum amplification from ground motion to beam orbit separation for a single transverse wave that propagates along the IR with no dissipation, for different wavelengths. For simplicity, this amplification is computed assuming that each quadrupole composing the IR is rigidly linked to the ground by its centre, and that each quadrupole moves parallel to the ground. The behaviour shown in Fig. 2 is compatible with the expectation knowing that, by definition, the phase advance along the quadrupoles of one IR triplet is close to zero, while the phase advance between the triplet on one side of the IP and the one on the other side is about 180 degrees. Therefore, one should expect:

- a net effect close to zero for wavelengths much larger than the whole IR region (i.e. $\lambda \gg 120$ m)
- a first amplification for a wavelength of approximately the length of the IR region (i.e. $\lambda \approx 120$ m)
- possibly higher amplification for wavelengths of the order of one triplet length (i.e. $\lambda \approx 35$ m) or lower.

The actual wavelengths and difference in pattern between LHC and HL-LHC cases, as shown in Fig. 2, is due to the actual distance between the triplet quadrupoles, that will slightly change in HL-LHC.

With respect to the values obtained in the uncorrelated case (Table 1), the fully correlated case gives about a factor two higher ground motion to orbit separation amplification for high frequencies. However, in the absence of strong, single-frequency, narrow-band excitation (as would be the case for a strong earthquake), the ground motion correlation quickly drops to zero over a short distance for frequencies above a few Hz [20,21]. On the contrary, for low frequencies, i.e. long wavelengths, the correlation can be preserved. In this case, the triplet or even the entire IR would move together as a whole, giving a zero net effect compared to moving each single element independently. In

[1] The main feature of the ATS optics configuration is the use of the matching quadrupoles in the adjacent IRs to support the β^*-squeeze in IP1/5. By that a lower β^* can be reached in IP1/5, with the cost of introducing a beta-beating wave throughout the arcs.

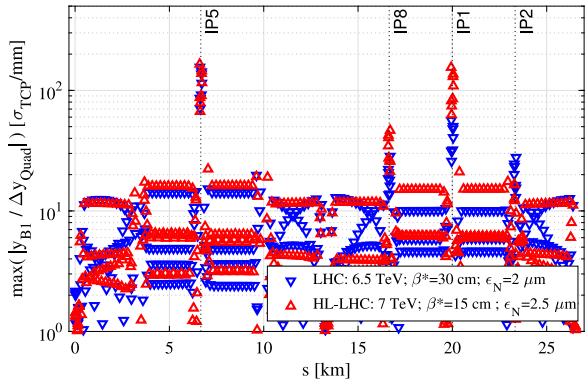

Fig. 3. Maximum vertical Beam 1 orbit variation at the primary collimators induced by the vertical displacement of each individual quadrupole in LHC (blue) and HL-LHC (red). The location of the IPs is highlighted. All values are given in rms beam sigmas at the primary collimator (σ_{TCP}) per mm of quadrupole rms displacement (Δy_{Quad}).

Table 2
Amplification factors (K_x and K_y, horizontal and vertical, respectively) between uncorrelated quadrupole motion and maximum orbit excursion at the primary collimators (TCP). All values are given in rms beam sigmas per μm of rms ground motion displacement.

	Beam 1		Beam 2	
	K_x	K_y	K_x	K_y
LHC all quads	0.4	0.4	0.5	0.4
LHC IR1/5 only	0.4	0.3	0.5	0.3
HL-LHC all quads	0.5	0.5	0.6	0.2
HL-LHC IR1/5 only	0.5	0.5	0.6	0.1

this regime, the uncorrelated estimates from Table 1 would even be overestimated.

Depending on the wave propagation speed (V), one can estimate the corresponding frequency as $f = V/\lambda$. The typical wave speeds measured in the CERN tunnels are 990 m/s for shear and 2200 m/s for pressure waves [4], which are compatible with measurements done elsewhere [22]. Taking 10 Hz as the frequency separation between the correlated and uncorrelated regimes [23], the corresponding wavelength would be about 100 to 200 m, which is of the order of the IR length. Therefore, in the absence of strong local ground motion sources it is unlikely to see the large amplification shown in Fig. 2 and the uncorrelated ground motion hypothesis seems to be most likely to be observed.

In conclusion, taking a conservative approach, one can set $K = 1$ for LHC and $K = 2$ for HL-LHC in Eq. (10) to obtain a conservative estimate on the threshold of the quadrupole rms transverse motion, for both horizontal and vertical planes, above which luminosity effects become noticeable (order of 1% luminosity drops in IP1 and IP5). With those assumptions and in terms of luminosity, LHC and HL-LHC are expected to tolerate up to 0.2 μm and 0.1 μm rms quadrupole motion, respectively.

3.2. Orbit excursion at collimators

Fig. 3 shows the amplification factor between each LHC/HL-LHC quadrupole displacement and the maximum Beam 1 (B1) vertical orbit variation at the primary collimator (TCP) [24,25]. Similar to the values presented in Table 1, the quadratic sum of the resulting orbit offsets at the TCP from all quadrupoles, assuming uncorrelated ground motion along the whole machine for each beam and plane, is reported in Table 2. Note that, as for the IP beam orbit separation, the orbit at the collimators is also dominated by the effect of the low-beta triplets, and that there will be a slight enhancement of sensitivity between the LHC and the HL-LHC.

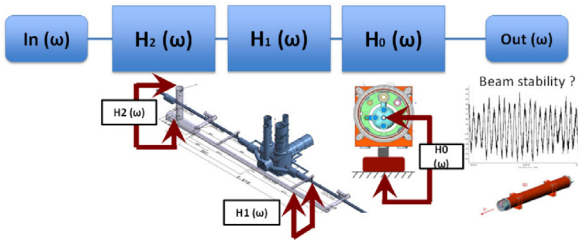

Fig. 4. Visualisation on how a combination of transfer functions can be used to estimate the beam response ($Out(\omega)$) from an input excitation signal ($In(\omega)$). The arrows indicate the points between which these transfer functions have been measured [6]. $H_1(\omega)$ and $H_2(\omega)$ give the horizontal (in LHC plane) and vertical (surface to LHC underground level) amplifications of the input signal through the surrounding ground. The direct ground-to-quadrupole cold mass response is given by $H_0(\omega)$, which has a vertical and horizontal component (not separated in the sketch).

On the other hand, one has to keep in mind that in the HL-LHC the total beam intensity will be about a factor of two higher than in the LHC. Therefore for a given orbit displacement at the collimators and assuming a comparable transverse beam distribution, the induced losses and the corresponding deposited energy could be at least a factor two higher in HL-LHC than in LHC. The actual particle distribution in the beam tails in LHC has been preliminarily assessed and results are summarised in Section 6.1.

4. Characterisation of ground motion

The oscillation of any accelerator component under the effect of ground motion depends on the characteristic spectra of the different sources of mechanical noise and on the mechanical transfer function between each source and the object itself. In general, a transfer function is defined as the ratio of the output of a system to the input of a system. In the context of this paper, the attention is on the ground-to-cold mass mechanical transfer functions of the accelerator quadrupoles. Assuming that one is interested in the vibration transfer from a source of ground motion located on the surface to the cold mass of a given magnet underground, the global transfer function $H(\omega)$ can be represented as a combination of its components:

$$H(\omega) = \begin{pmatrix} H_x(\omega) \\ H_y(\omega) \end{pmatrix} = \begin{pmatrix} H_1(\omega) \\ H_2(\omega) \end{pmatrix} \cdot \begin{pmatrix} H_{0,x}(\omega) & H_{0,y}(\omega) \end{pmatrix} \tag{11}$$

where $H_0(\omega)$, which has a component in horizontal and vertical direction, is the transfer function between the magnet's magnetic centre and the slab on which the magnet is placed. $H_1(\omega)$ and $H_2(\omega)$ describe the vibration transfer through the ground horizontally within the LHC plane and vertically from the surface to LHC underground level. In Fig. 4 a visualisation of the components to obtain a signal transfer from the source of the vibration to the beam location is shown.

$H_1(\omega)$ and $H_2(\omega)$ have been measured around LHC IP1 [6] between the locations indicated by the arrows in Fig. 4. They depend on the distance between source and observation point and on the exact ground formation in between. Since the ground structure to any possible source point is in general unknown, a measurement of these transfer functions can only give an indication of the amplification. The accuracy of estimates is therefore improved, if the ground motion can be measured in the tunnel close to the magnet. In that case the required transfer function reduces to $H(\omega) = H_0(\omega)$. As it will be shown in Section 4.1, the ground motion is measured close to the triplet quadrupoles within the LHC tunnel, therefore $H_0(\omega)$ is the only transfer function relevant for the presented analysis.

The response of the system $R(\omega)$ to a single input can be computed as

$$R(\omega) = |H(\omega)|^2 \cdot f(\omega) \tag{12}$$

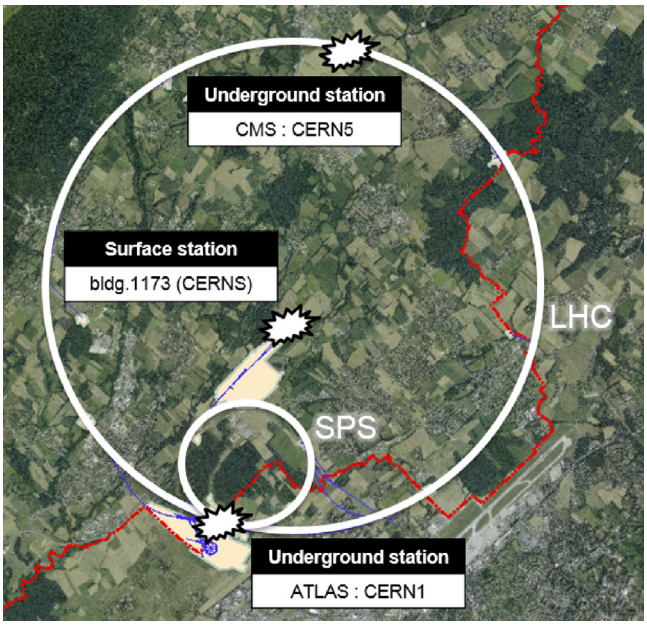

Fig. 5. Overview of CERN accelerator complex with CERN Seismic Network station locations.

where $f(\omega)$ is the Power Spectral Density (PSD) input from ground motion measurements. The rms motion at the response point can then be calculated as

$$R_{\text{rms}} = \left(\int_0^\infty R(\omega) d\omega \right)^{1/2}, \tag{13}$$

The input PSD $f(\omega)$ can be obtained by measuring the frequency spectra of the ground motion during a given period of time, e.g. by geophones. In general, $R(\omega)$, $f(\omega)$ and R_{rms} have horizontal and vertical components that are evaluated independently.

4.1. CERN Seismic Measurement Network

The official CERN Seismic Network began its constant monitoring in March 2017 [26] in collaboration with the Swiss Seismological Service (SED) [27]. The aim of this network is to provide an overview of the seismic activity in the proximity of the LHC. In total three seismic stations were installed: one is located on the surface approximately in the centre of the LHC ring, the other two are placed about 100 m underground close to the low-beta triplet quadrupoles adjacent to IP1 and IP5. An overview of the sensor locations is shown in Fig. 5. Each station is equipped with both broadband and strong-motion seismometers as described in Ref. [5]. Since March 2017, the CERN seismic network is in continuous operation and publishes its measured data to the "C4" network designation of the SED, making it publicly accessible from the web.

The network was designed to be compatible with the harsh environment in the LHC tunnel. It is able to track the ground motion in a range of 0.03–100 Hz, with amplitudes ranging from the quiet underground motion up to $2g$, where $g = 9.81\,\text{m/s}^2$ is the gravitational acceleration. This wide range of measurements allows to get an accurate feedback on the ground stability in the LHC tunnel.

While the main purpose of this system is to record the human-made noise induced by CE in the LHC tunnel, it also catches earthquakes originating from all around the world. Fig. 6 shows an example of the strongest local earthquake event in the Geneva lake area in 2018 that was recorded in all three CERN seismic stations.[2] This example shows that a signal from the same seismic source can be received quite differently over the distance of the LHC circumference. The signal is measured in velocity (top) and converted into displacement (bottom) by integration.

The first year of data taking was used to collect reference measurements without any CE work related to HL-LHC construction. Once CE works began in spring 2018, the seismic activity in the LHC tunnel was monitored constantly. Fig. 7 shows a typical PSD in the horizontal plane measured at the three locations indicated in Fig. 5 (IP1, IP5 and surface) not affected by CE. In order to quantify the impact on LHC operation from an early stage, a warning system was setup to trigger when the vibration levels exceeded a predefined threshold. As will be detailed in the following chapters, on many occasions these warnings were triggered and clear effects were visible on the LHC beam.

4.2. Ground-to-magnet transfer function

Depending on the support structure that connects the magnet to the ground and how the cold mass is carried by the magnet's outer shell, different magnets will in general have different transfer functions. As described in Section 3, the most sensitive magnets are the low-beta triplet quadrupoles next to IP1 and IP5 where the beta-functions are the largest and cause the largest orbit excursions for a given cold mass displacement. Thus, the knowledge of the triplet transfer function is the most relevant.

The $H_0(\omega)$ measurement of a magnet is performed by placing accelerometers inside the cryostat, two at the extremes of the magnet's cold mass and one inserted in the middle of it, plus sensors placed on the ground near the supporting feet. An external perturbation is applied using a hammer to hit the ground at a certain distance. The response of the magnet to the perturbation is measured and a spectral decomposition is performed to extract the sensitivity to different frequencies.

At the time of writing, two transfer function measurements performed on LHC spare magnets were available. The first one was performed in 2017 on a LHC Q1 final-focusing quadrupole [6]. This particular magnet is a spare for the first quadrupole within a low-beta triplet assembly. This magnet was chosen for the measurement because it best represents the LHC triplet magnets around the high luminosity experiments. Fig. 8 shows the measured horizontal and vertical transfer functions for this magnet, measured on a stand-alone assembly in a surface building and averaged over the three sensors along the magnet. Several peaks are visible that correspond to the natural oscillation frequencies of the magnet, the main ones around 21 Hz in the vertical plane.

The structure and support of the HL-LHC triplet cryo-assembly has been changed from that of the LHC triplet and will be similar to the one of the LHC dipole. Fig. 9 shows the simulated amplification factor for the LHC arc dipole and HL-LHC quadrupole as a function of the excitation frequency in the horizontal (top) and the vertical plane (bottom). The simulations have been obtained by a finite element analysis of the mechanical design of those magnets assuming a 1% overall damping ratio [28]. The two magnets are clearly different in terms of simulated transverse response, however the number and amplitude of the main resonance frequencies are comparable, which is expected from the compatibility of the mechanical assembly.

At the time of writing, no fully cryostated HL-LHC triplet quadrupoles exist. Therefore, in order to validate the accuracy of the simulation of $H_0(\omega)$, a new measurement was performed on a LHC dipole cryo-assembly in 2020, using the same ground support configuration foreseen for the new triplet. The measurement setup and installation of the geophones were similar to the 2017 measurement of the LHC triplet quadrupole. Five measurements were taken in both the vertical and the horizontal direction using the natural ground motion observed in the test building. The results (averaged over the three measurement locations along the magnet) are shown in Fig. 10. In

[2] The surface station is not shown in Fig. 6 due to a problem with the recording for this event.

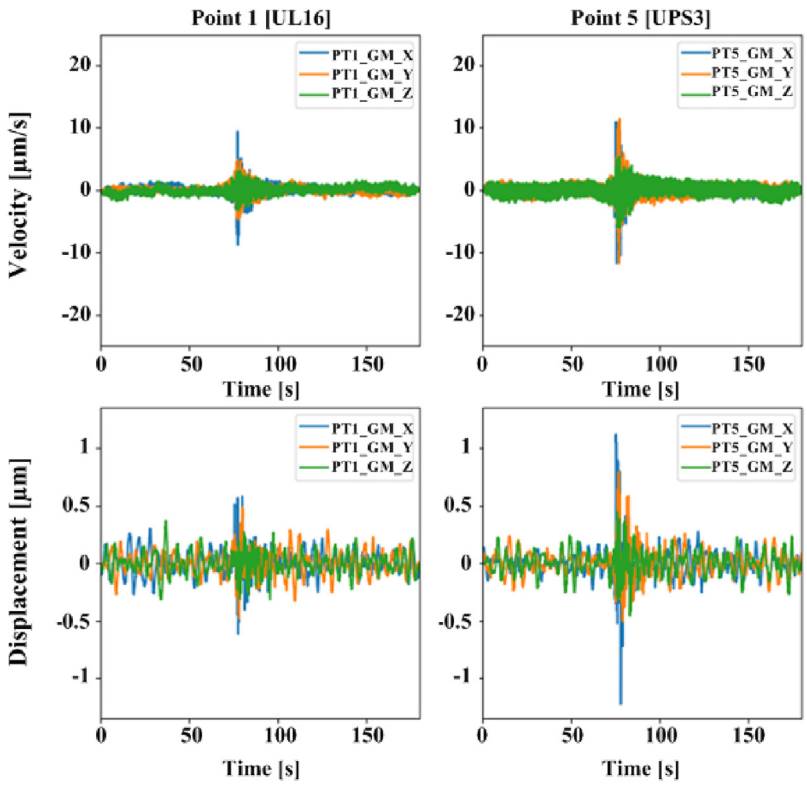

Fig. 6. Strongest local earthquake event in the Geneva lake area in 2018 with the LHC beam present: 29 September 2018 6 h 30 (UTC time), magnitude 2.6, epicentre located at Thonon-les-Bains, France, 35 km from ATLAS experiment. The plot shows 3 min of data at the two underground stations in IP1 (left) and IP5 (right). The three lines show the measurement in each plane. The coordinate systems refers to the beam orbit: Y correspond to the vertical direction, X points horizontally ring outward and Z in beam directions.

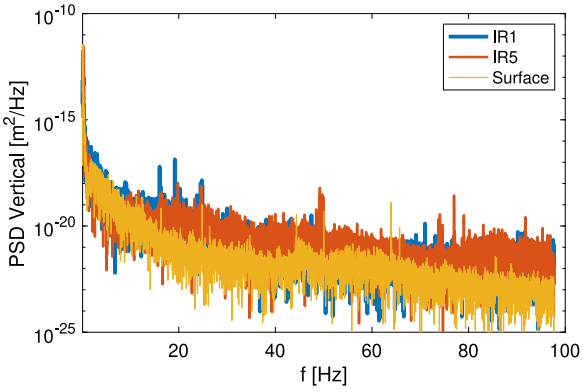

Fig. 7. Power spectral density (PSD) in the horizontal plane measured at CERN in the three locations that are shown in Fig. 5.

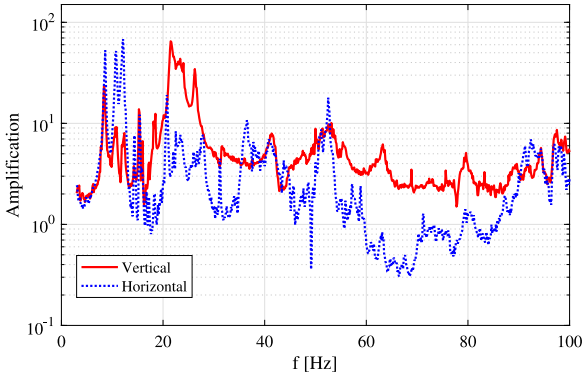

Fig. 8. Measurement of $H_0(\omega)$ the mechanical magnet transfer function in the horizontal and vertical plane for the LHC Q1 quadrupole.

each case the amplification factor is represented as a function of the excitation frequency. The results of the simulations (blue line) that were shown in Fig. 9 are overlaid again for comparison. In the vertical plane the main peaks observed in the simulation are represented in the measurement with a compatible magnitude. The exact position and width of resonant peaks strongly depends on the actual geometry and the stiffness of the magnet anchoring to the ground. The observed mismatches are believed to be introduced by the limited accuracy of the simulation model. In the horizontal plane the results show several peaks not represented by simulations. This might be due to the fact that the measurement in the radial direction is more delicate than in the vertical plane and that some coupling between radial and vertical planes may appear. The differences observed are considered to have a minor impact to the results presented in this paper. When discussing expectations for HL-LHC performance in Section 6, Fig. 21 will show that the measured ground motion amplified by the different transfer functions from Figs. 8–10 result in similar baseline triplet motions while the largest excitation peaks are as well seen with each amplification function. Especially the simulated and measured LHC dipole amplification functions (Fig. 10) give compatible results.

Measurements on an actual HL-LHC triplet magnet are foreseen when it becomes available to validate the presented estimates.

5. Observation of ground motion on LHC beams

Fig. 11 shows the typical rms ground motion measured in the underground structures close to IP1 integrated over a series of frequency bands along a fill in 2017. The variation in the frequency range from 1 to 10 Hz is a consequence of the different noise levels between day and night.

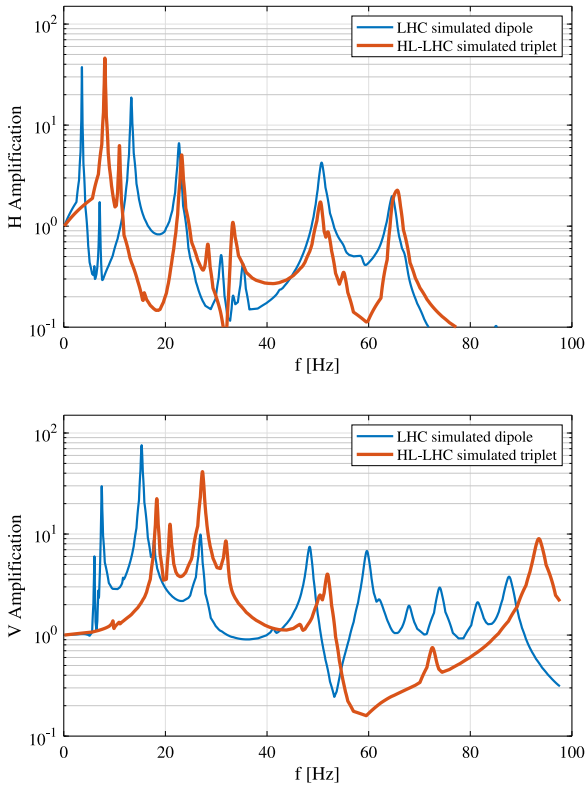

Fig. 9. Comparison of the simulated transfer function between the LHC dipole and the HL-LHC triplet magnets in the horizontal (top) and vertical (bottom) plane [28].

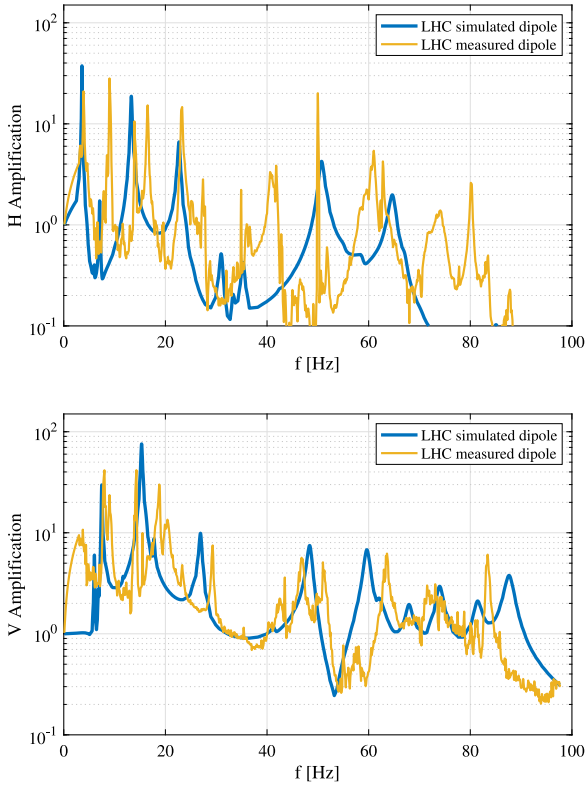

Fig. 10. Measured transfer function (yellow) in the LHC main arc dipole in the horizontal (top) and vertical direction (bottom). The simulated LHC dipole curve (blue) from Fig. 9 is again overlaid for comparison.

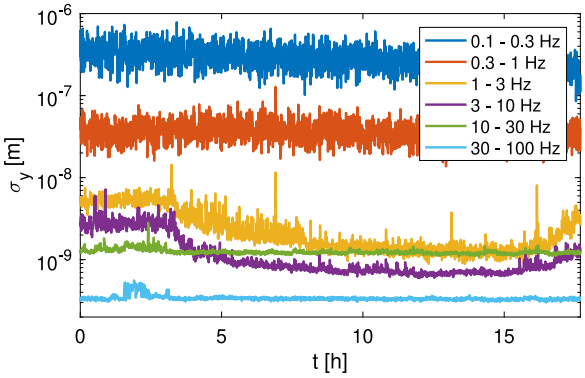

Fig. 11. Measured vertical ground motion underground close to IP1 integrated over different bands of frequency as a function of time from the start of a typical LHC fill. The drop in the frequency range from 1 to 10 Hz arises from the different noise levels between day (~6:00–18:00) and night.

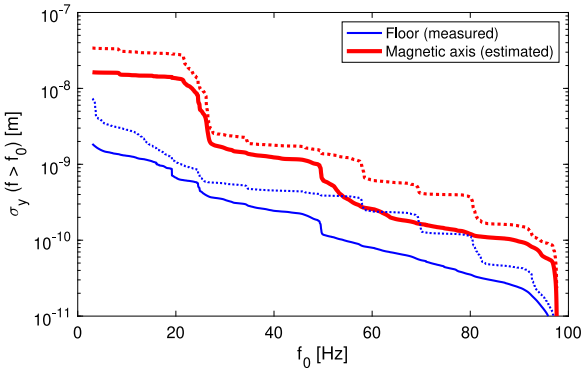

Fig. 12. Integrated PSD of the mean (solid) and max (dashed) ground motion measured in IP1 during a typical LHC fill on the floor (blue), and after applying the cold mass amplification shown in Fig. 8 for $f > 3$ Hz (red).

Table 3
Expected maximum rms beam orbit separation at the IP, consequent luminosity loss and orbit offset at the collimators for uniform and uncorrelated ground motion of 0.04 μm rms.

	LHC	HL-LHC
Orbit separation at IP1/5 [σ_{IP}]	0.01	0.03
Luminosity loss [%]	<0.1	<0.1
Orbit offset at TCPs [σ_{IP}]	0.01	0.02

As explained in Section 4.2, the amplification between ground motion and magnetic centre motion of a spare LHC Q1 magnet has been measured for frequencies above 3 Hz [6]. We assume that the motion at frequencies below 3 Hz belong to the correlated regime that should have a much lower impact (see Fig. 2) and/or would be taken care of by the present orbit feedback system.

With the assumption of fully uncorrelated ground motion, this can be used to estimate the effective motion of the quadrupole axis. The blue curve in Fig. 12 shows the integrated PSD of the ground motion measurement in the LHC tunnel,[3] the red curve estimates the movement of the magnetic axis by applying the measured amplification (as shown in Fig. 8) to the blue curve in Fig. 12. From this estimation the expected rms vertical motion of the triplets should be below 0.04 μm. In such a condition and by considering the amplification factors in Tables 1 and 2, and using Eq. (7) to compute the expected luminosity reduction, one obtains the values in Table 3.

[3] The quiet underground spectra measured close to IP1 and IP5 are very similar and provide compatible results in terms of integrated PSD.

During the fill under analysis the measured luminosity and orbit variation at the primary collimators did not show any visible impact of ground motion. The values in Table 3 represent the amount of beam separation at the IP, luminosity loss and orbit offset at the TCPs that can be expected from daily ground motion during operation without any special excitation events.

5.1. Earthquakes

Earthquakes are rare events. How they arrive at the LHC depends on their magnitude and distance travelled from the epi-centre. The beam response and potential resonant amplification of the induced ground movement by (parts of) the LHC elements depends on the propagation direction and wavelength. Many such events were observed on the LHC beams during different parts of the operational cycle. Most earthquakes with magnitude above 7 occurring anywhere on the planet are routinely observed on the LHC beams. Effects were measured over timescales from a few seconds up to one hour and with varying impact. The main observables are orbit changes and beam loss signatures on the primary collimators, but they can also be seen as a variation of the luminosity, if the event happens during the collision period. An example of the radial oscillation of the LHC ring induced by the pressure waves from a magnitude 8 earthquake is shown in Fig. 13.

Since earthquakes are rare events and feature excitation only at low frequencies (<1 Hz), they do not impose a performance risk to (HL-)LHC. Whether beams would be dumped for a certain orbit movement strongly depends, among other things, on the tail population, wave properties, collimator and BLM dump threshold settings. So far no beam dump was caused by such an event in the LHC. Nevertheless, roughly scaling the observed loss patterns at the TCP, indicates that some events could have dumped the beam under HL-LHC conditions.

Because of their clear signatures on the LHC beams, earthquakes constitute an interesting benchmark case for simulation tools and help to correlate ground motion with observations on the different beam measurement devices and identify observables for other ground motion studies.

5.2. Civil engineering works

Already in 2015–2016, a study was performed to characterise the impact of different civil engineering machines on an LHC magnet based on a transfer function approach. Fig. 14 shows the first part of this study, where the induced vibration of several heavy CE machines is characterised as a function of excitation frequency along with the vibration level in the underground cavern of the CMS detector (grey), where the effects of human-made ground motion is strongly suppressed. This data was confirmed in LHC Long Shutdown 2 (LS2, 2019–2020) during the excavation of shafts, tunnels and galleries for the HL-LHC project with the use of different types of machines [6].

During the whole period from April to December 2018 several types of CE work were performed in parallel to LHC beam operation, using a variety of tools inducing vibrations in different frequency ranges. Beam observables, such as orbit, luminosity, beam intensity and losses were analysed in comparison to ground motion activity especially when a warning was triggered, see Section 4.1. Particularly for this purpose the existing instrumentation of the transverse dampers (ADT) [29,30] and the Beam Position Monitors (BPM) with DOROS readout [31] were extended to capture and log beam spectra, allowing the ground vibration frequencies amplified on the beam to be better investigated.

The ground motion spectra are calculated from the position data over one minute periods and are logged three times per minute. The ADT spectra are calculated from position data of the first 10 s of each minute and therefore contain only snapshots of every sixth 10 s window. The partial time coverage of the ADT data has to be kept in mind when comparing this data to ground motion spectra, because certain effects might not be detected in the ADT data or may appear less evident.

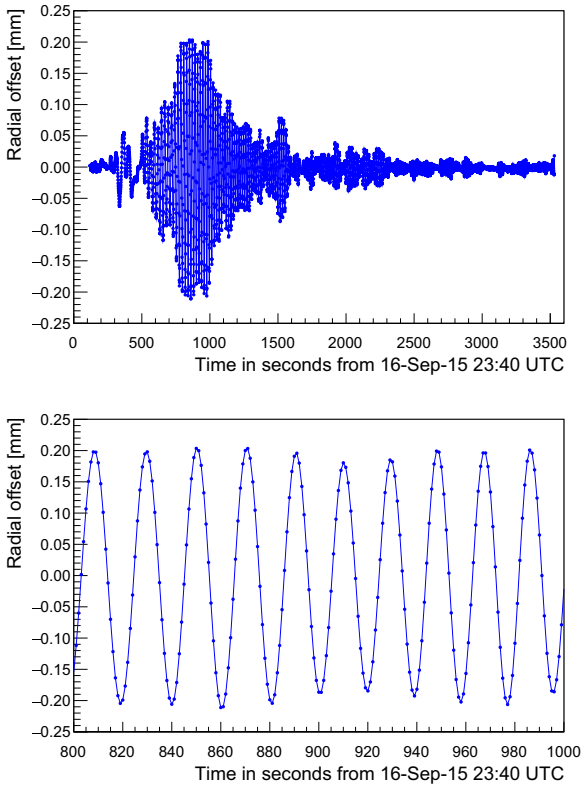

Fig. 13. Radial excursion of the beams (average over arc BPMs) during the passage of the pressure waves resulting from a magnitude 8.3 earthquake in Chile on 15 September 2015. The LHC machine was at injection energy during this period. The waves took roughly 1 h to travel from Chile to Geneva. The lower plot shows a zoom on the period with largest amplitude, revealing a regular oscillation with a period of 20 s.

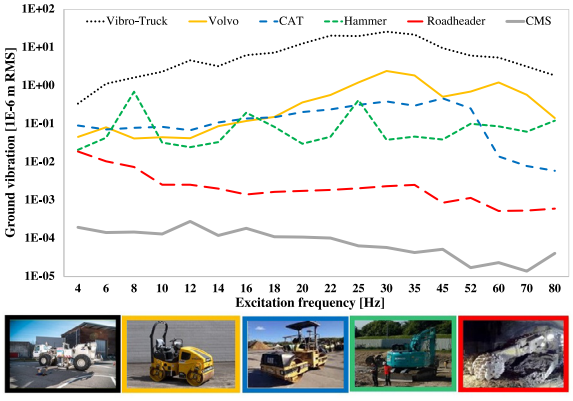

Fig. 14. Characterisation of the vibration induced by several heavy CE machines in comparison to (quiet) underground levels close to the CMS experiment (grey) [10]. Note the orders of magnitude difference in ground vibration levels for the selected machines. "Vibro-Truck" (top dotted black line) refers to a vibration truck that excites controlled frequencies with a well defined amplitude, it is used as a reference vibration source to study the frequency response of the ground. The horizontal axis uses octave band binning.

Fig. 15 shows the rms ground motion and ADT beam spectra measurements within four selected frequency bands during LHC luminosity production in 2018. Compressing the individual frequency information into the rms of a frequency band helps to quickly identify when ground motion activity is picked up by the beams. Once correlations are identified, the full spectra and beam evolution data are investigated in detail (the next section gives an example for LHC fill number 6757).

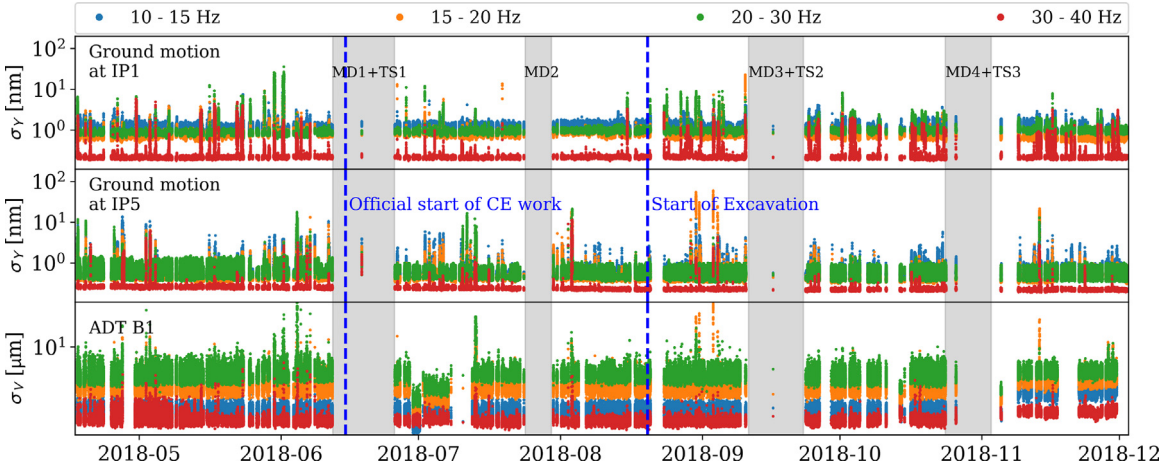

Fig. 15. Ground (top: IP1, middle: IP5) and beam motion (bottom from ADT located in IP4) rms obtained from integration of spectra over selected frequency bands. Only data with colliding beams (*Stable Beams*) in 2018 is shown. The longer data gaps are due to machine development (MD) experiment periods and technical stops (TS). The official HL-LHC ground breaking and the start of shaft excavation are indicated by blue dashed vertical lines.

The presented analysis focuses on the vertical plane, since CE activity primarily excites vertical ground vibration [32], and thus this is the main direction in which the triplet quadrupoles will react and transmit the movement to the beam.

Only frequency ranges between 10–40 Hz are shown. This is a critical frequency range for two reasons. Firstly, the amplification from ground to cold mass vibrations of a triplet quadrupoles has strong vertical modes around 21 Hz, while horizontal amplification is stronger at lower frequencies around 10 Hz (see [6] and Section 4.2). Secondly, CE machinery, e.g. ground compactors, operate close to these triplet eigenmodes [6] and can therefore lead to resonant excitation.

Ground and beam excitation is observed in all four frequency bands displayed in Fig. 15. However, only a few ground motion events are highly amplified on the beams. Some events show activity over all bands, others clearly excite only distinct frequencies. The strongest and clearest events seen on the beams were generated in IP5 in the frequency range between 15–30 Hz (green and orange). These excitations lasted several minutes.

In general, in IP5 frequencies between 10–20 Hz seem to be most commonly excited, while in IP1 activity at higher frequencies between 20–40 Hz are more often observed. This can be explained by the different equipment that has been used at the two sites.

The ground movement observed in the frequency range 1–10 Hz[4] is correlated in all three data sets (ground motion in both IPs and ADT). HL-LHC CE work in IP1 and IP5 will lead to ground motion signals limited to their source location. Only stronger or more global, e.g. natural, sources will lead to correlated signals in both IPs, which is not the concern of the presented analysis. Ground activity in the range 40–100 Hz[5] was recorded with high amplitudes especially in IP1 from mid August. The effect on the beam was however mild to negligible. Both outer frequency ranges have a low amplification from ground to cold mass (see transfer function measurements and simulations in Figs. 8–10) and are therefore less critical.

5.3. Example: Fill 6757

During the first period of the CE campaign, when surface work using compactors were performed in IP5, some of the strongest reactions of the circulating beams were observed. Compactors compress the ground by vibrating in a variable frequency range around 20–30 Hz. The triplet is very sensitive to these frequencies because of the proximity to its eigenmodes.

[4] Not shown in Fig. 15.
[5] Not shown in Fig. 15.

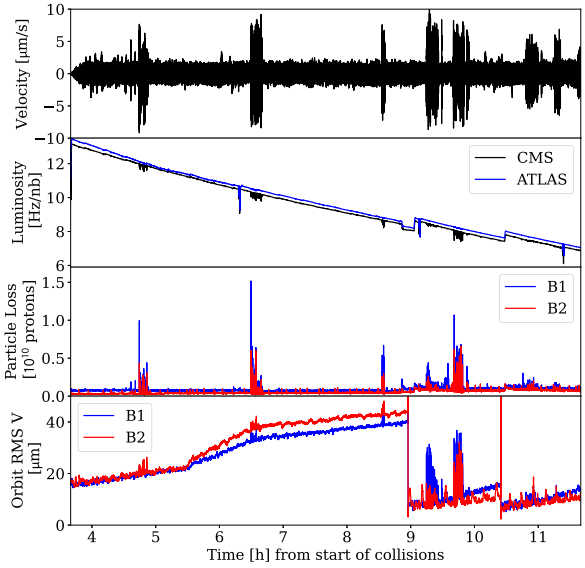

Fig. 16. Seismic activity in IP5 (top row) and beam evolution during Fill 6757 (4 June 2018). 2nd to 4th row: ATLAS and CMS online luminosity, calibrated losses on primary collimator, vertical rms orbit. Several ground excitation periods are clearly visible on each data set. The orbit rms is calculated with respect to the operational orbit feedback reference, defining the rms to zero when taken at the beginning of collisions at $t = 0$ h. At $t = 8.9$ h and $t = 10.3$ h a β^*-levelling step was performed in IP1 and IP5, before which the orbit reference was updated, resulting in the rms going back to zero. The short luminosity dips at $t = 6.2$ h, 9.1 h and 11.3 h are induced by luminosity optimisations.

Fig. 16 shows the time evolution of several key observables on the example Fill 6757 (4 June 2018). The seismic activity measured underground close to the IP5 triplet quadrupoles (top row) shows several clear vibration periods that were transmitted with varying impact to the LHC beams (bottom three rows). The CMS luminosity dips down by up to a few percent and the beam losses on the primary collimators and the rms of the vertical beam position around the ring increase on both beams. Even though the beams had a considerable reaction to the CE work, the highest loss spike only reached about 5% of the beam abort threshold.

The ground vibrations are of similar amplitude for the first five excited periods, while at $t = 4.7$ h, 6.5 h, 8.6 h and 9.7 h the luminosity dips and beam losses are much stronger compared to $t = 9.2$ h. This varying reactions of the beam to excitation of similar strength can be explained by the frequency content of the ground movement as

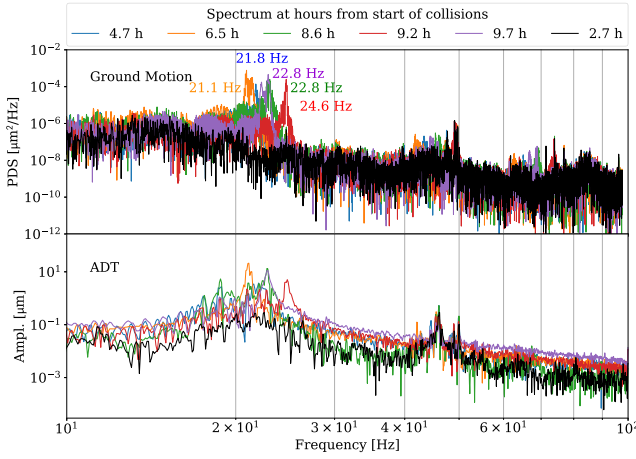

Fig. 17. Ground motion (top) and beam (from ADT, bottom) spectra during five CE working periods, showing the changing ground excitation frequency and its presence on the beam. Black: reference measurement without CE excitation.

illustrated in Fig. 17. This figure selects individual spectra out of the mentioned periods in Fig. 16. The black line shows a reference spectrum during a calm moment without CE work. The red spectrum, recorded at $t = 9.2$ h, excited around 25 Hz and had only very little impact on the beam. The orange, green and purple lines, recorded at $t = 6.5$ h, 8.6 h and 9.7 h and exciting around 21–22 Hz, had the largest effect on the beam, since these almost exactly hit the triplet resonance at 21 Hz. The two periods around $t = 10.5$–11.5 h feature about half the seismic amplitude and excite around 30 Hz, with the effect on the beam hardly above the noise level.

Similarly to Fig. 15, where the rms of the floor motion is obtained from an integration of the measured ground motion spectra, Fig. 18 estimates the triplet quadrupole motion in IP5. The measured ground motion PSD is amplified by the measured triplet transfer function (as shown in Fig. 8) to estimate the corresponding magnet motion PSD before the integration over selected frequency bands provides the rms quadrupole motion. This calculation is performed for all spectra over the full duration of Fill 6757. From the optics model, the triplet offset leading to a 1% luminosity loss is calculated in Section 3 and indicated as the red dashed line in Fig. 18. The four periods at $t = 4.7$ h, 6.5 h, 8.6 h and 9.7 h exceed this 1% luminosity-loss threshold, which is in good agreement with the luminosity data measured by CMS as shown in Fig. 19.

Figs. 18(bottom), 19 and 20 show zooms to the strongest excitation event at $t = 6.5$ h. The observed beam motion close to IP5 (Fig. 20(top)) and at the primary collimators (Fig. 20(bottom)), as well as the luminosity evolution measured by CMS (Fig. 19) are compared to the expectations calculated from the observed ground motion in combination with the measured transfer functions (see discussion in Section 4.2). The expectations show a good qualitative and quantitative agreement to the data, which gives confidence for the validity of the model when scaled to HL-LHC conditions.

6. Expectations for HL–LHC

The measured transfer function along with the measured PSD during a particular time can be used to evaluate the impact on the actual magnet motion and how this translates into luminosity loss. In Fig. 21 the expected magnet motion is shown as the convolution of the different transfer functions (measured or simulated) and the ground motion recorded during the 2018 operational run (which includes several peaks associated to the civil engineering works carried out in parallel to the LHC operation). The expected motion is well below the 1% luminosity loss threshold represented by the red dashed horizontal

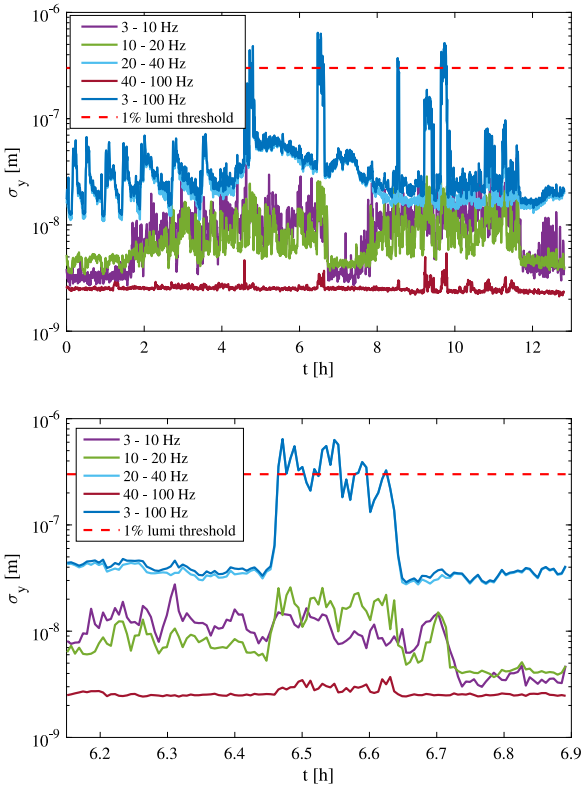

Fig. 18. Top: Estimated rms triplet magnetic axis motion during fill 6757 introduced by ground motion in the selected frequency bands. Red dashed line represents the value for which a 1% luminosity loss is estimated for LHC as computed in Section 3. Bottom: Zoom to the strongest excitation event at $t = 6.5$ h when the motion exceeded the 1% luminosity-loss threshold.

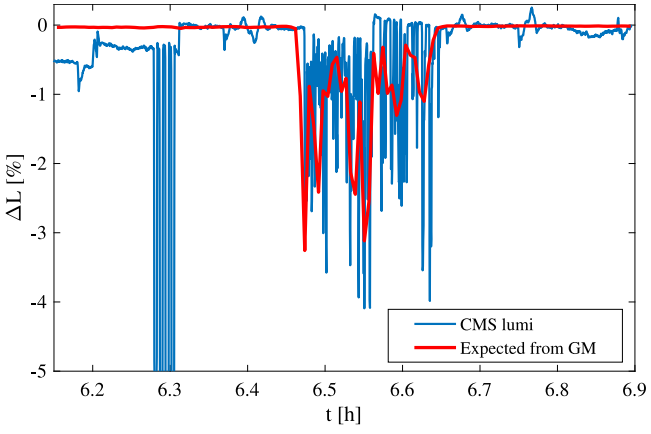

Fig. 19. Luminosity spikes (slow exponential decay subtracted in the plot) detected by CMS during the strongest excitation event of fill 6757.

line. Therefore, it can be concluded that ground motion is not expected to impose strong limitations in the future HL-LHC instantaneous luminosity performance.

On the other hand, sudden movements of the beam orbit at the collimator might lead to losses that could trigger beam dumps and therefore strongly impact the integrated luminosity. This aspect calls for additional considerations on the tail population, which are described in the following section.

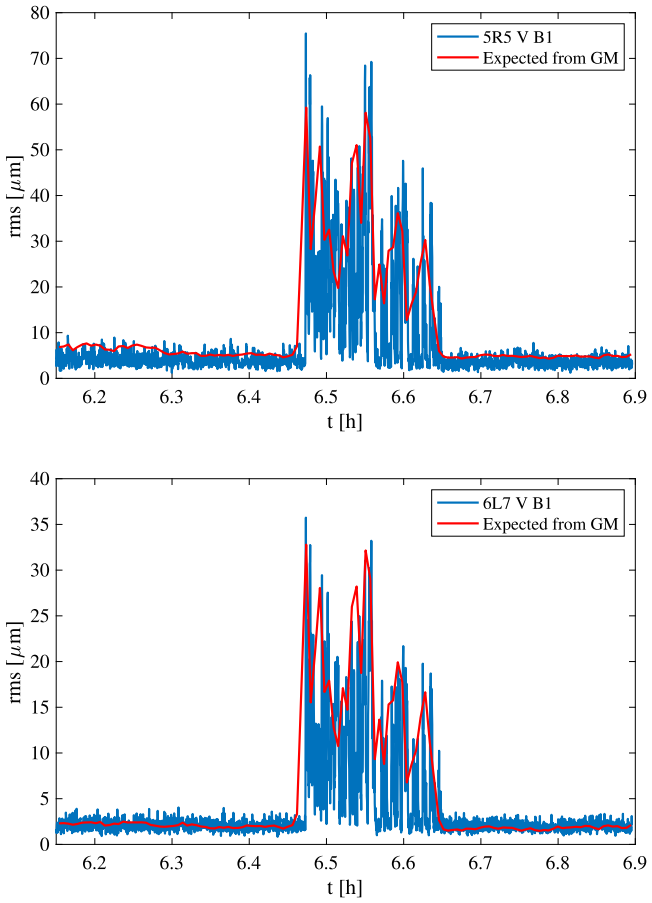

Fig. 20. Vertical orbit measured during the strongest excitation event of fill 6757 for Beam 1, top: at the most sensitive BPM of the ring (with respect to motion of triplets, located in cell 5 right of IP5), bottom: at the primary collimators (BPM located in cell 6 left of IP7).

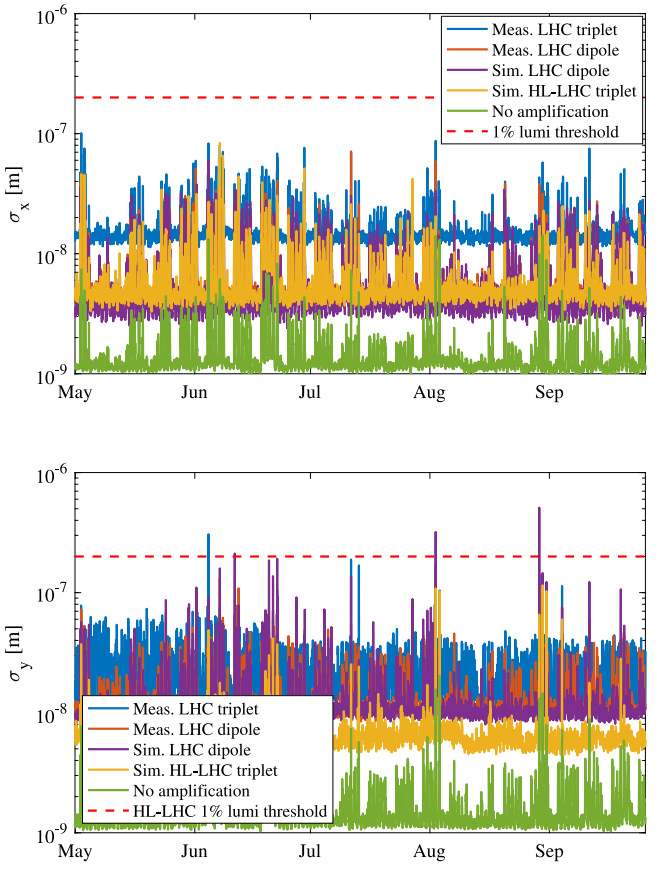

Fig. 21. Projected magnet movement in the horizontal (top) and vertical plane (bottom) induced by ground motion and considering different transfer functions. Red dashed line represents the value for which a 1% luminosity loss is estimated for HL-LHC as computed in Section 3.

6.1. Beam tail population

The total energy stored in the HL-LHC beam will be of about 700 MJ. Even a small fraction of the beam lost in the superconducting regions may induce a magnet quench. For that reason, it is of particular interest to determine the beam tail population since this will be the region most likely to suffer from beam scraping at the primary collimator (TCP). From past experience [33], it is known that the transverse beam distribution is not a perfect Gaussian, but rather a composition of two Gaussian distributions, one representing the core and another one representing the tails. This double-Gaussian distribution is given by,

$$\rho(x) = \frac{I_1}{\sqrt{2\pi}\sigma_1}\exp\left(-\frac{x^2}{2\sigma_1^2}\right) + \frac{I_2}{\sqrt{2\pi}\sigma_2}\exp\left(-\frac{x^2}{2\sigma_2^2}\right). \tag{14}$$

The tail population has been investigated in dedicated measurements using controlled collimator scraping [34]. Those investigations could only be performed either at injection energy or at high energy with a single bunch, and therefore with conditions far from nominal colliding beams. Moreover, it is not clear whether the LHC beam distribution will be representative for HL-LHC. Nevertheless, since this is the only experimental evidence available to make a guess on the beam distribution, it is used to estimate the number of protons scraped on the TCP by a ground motion induced orbit offset.

Based on the available measurements, here it is assumed that $\frac{I_1}{I_2} = \frac{65}{35}$ and $\sigma_2 = 2\sigma_1 = 2\sigma$ in Eq. (14). A graphical representation of the resulting distribution is shown in Fig. 22. To determine the fraction of the beam that might potentially be scraped an estimate of the maximum expected orbit jitter at the TCP is required. As shown in Table 3, the maximum orbit offset at the TCP expected from ground motion is 0.02σ rms in the case of the HL-LHC. From the model of the tail population in Eq. (14), the number of protons stored in the region between the collimator cut n_{TCP} and $n_{\mathrm{TCP}} - n0.02\sigma$, can be estimated, where n is the margin factor considered to estimate the maximum displacement. In this study $n = 3$ is set, which represents a maximum orbit at the TCP of about 100 μm. According to the collimator specifications for the HL-LHC [35], the collimator cut will be set to $n_{\mathrm{TCP}} = 6.74\sigma$ for a beam emittance of $\epsilon_n = 2.5$ µm. Performing the integral of Eq. (14) within the integration limits explained above and taking into account the rotation of the phase space, the fraction of the beam that is scraped can be obtained:

$$\frac{N_p}{I_b} = 2\int_{(6.74-0.06)\sigma}^{6.74\sigma} \rho(x)dx = 3\cdot 10^{-5}. \tag{15}$$

In absolute terms, for a beam intensity of $I_b = 6.35\cdot 10^{14}$ protons (assuming HL-LHC 2760 bunches of $2.3\cdot 10^{11}$ protons per bunch [18]), this computes to $1.9\cdot 10^{10}$ scraped protons.

Comparing this result to the present LHC dump threshold for fast losses (10 ms) at the TCP, which is of the order of $1\cdot 10^{11}$ lost protons [36], this would correspond to about a factor five below the given dump threshold. However, as stressed before, these numbers strongly depend on the tail population measurement results, which might vary with beam conditions and it is unknown to what extend those actually describe the HL-LHC physics beams.

Also note that the fastest orbit jump observed so far is about 10 ms [37], but such jumps correspond to magnet failures just before the beams are dumped or to transients during beam dumps. No fast

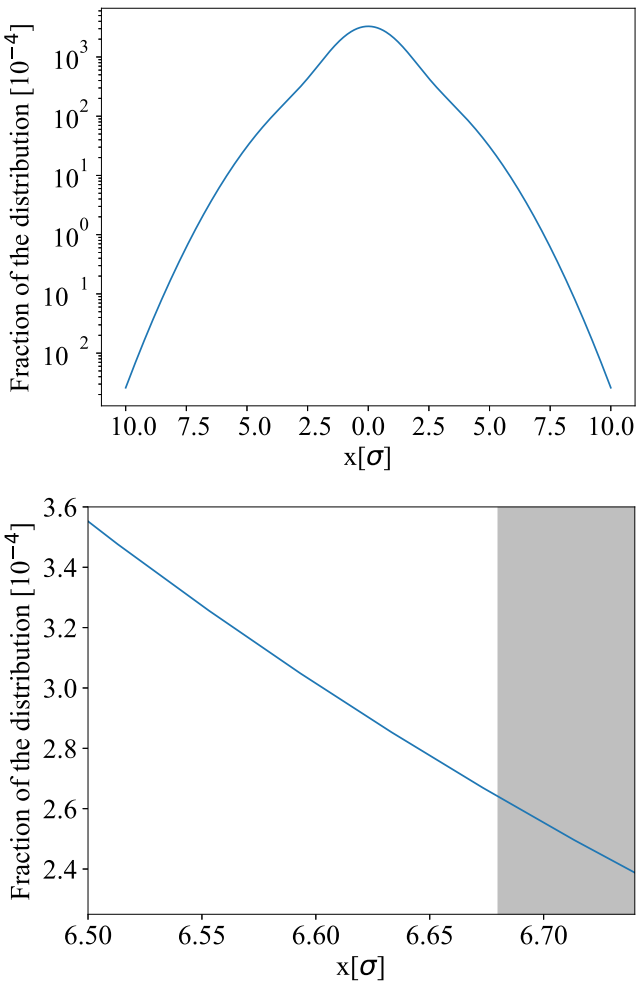

Fig. 22. Double-Gaussian distribution. This model is used to estimate the number of particles scraped due to orbit jitter. In the bottom plot the estimate of the scraped area (grey) is shown.

transient of the orbit due to ground motion was ever observed at the LHC on the millisecond time scale. The fastest orbit transients that have been observed on the 0.1 second time scale were due to orbit oscillations at frequencies close to 10 Hz.

The estimates made in this section should underline how difficult it is at the present stage to draw conclusions on the dump potential and performance reduction from ground motion excitation for the HL-LHC. Assumptions must be made on the transverse beam distribution as well as on the collimator settings and dump thresholds. Especially the knowledge of the tail population is highly uncertain, but crucial to obtain a meaningful result.

7. Conclusion and outlook

Ground motion effects on the LHC beam orbit and their impact on performance have been studied since the accelerator's design phase (e.g. in [2–4,11,23,38,39]). In this paper we use recently developed monitoring options to study and compare ground excitation from different sources (perpetual ground motion, earthquakes, civil engineering) and look at their effects on the LHC and HL-LHC beams.

In preparation for the installation of HL-LHC equipment in Long Shutdown 3 (LS3), civil engineering (CE) work, like building surface infrastructure and excavating new shafts, have been executed close to the two low-beta interaction points IP1 and IP5 from June 2018 in parallel to LHC beam operation. In view of this HL-LHC CE work, the CERN seismic measurement network started operation in 2017 with three seismic sensors installed in critical locations. A warning system has been put in place to trigger an alarm in case the measured ground motion close to the LHC triplet magnets exceeds predefined thresholds. On multiple occasions this alarm was triggered by ground motion linked to the CE surface activity. These events caused orbit disturbances, beam losses and luminosity dips of the order of a few percent. The effects were however hardly noticeable during daily LHC operation. No premature beam dumps were induced. The reaction of the beams strongly depends on the frequency content of the exciting ground vibrations. The surface work with ground compactors around IP5 had the most significant impact as they excited at frequencies around the triplet eigenfrequency of 21 Hz.

The HL-LHC triplet quadrupole ground anchoring will be similar to that of the current LHC main dipole. Since a fully cryostated HL-LHC triplet magnet is not yet available, transfer function measurements using a spare LHC arc dipole have been carried out and compared to a preliminary simulation of the HL-LHC triplet transfer function. The results show a reasonable agreement, which allow this data to be used for scaling between the LHC and the HL-LHC.

Based on these triplet transfer functions and optics simulations, a model was developed that is able to quantitatively reproduce the observed orbit and luminosity effects induced by a given ground motion signal. After validation with LHC data, this model was used to estimate the impact of ground motion on the HL-LHC beam performance.

The presented analysis shows that the HL-LHC will be approximately a factor 2 more sensitive to ground motion than the LHC. The IP1/5 triplets are the most critical elements and cause the largest orbit disturbance when vibrating. Nevertheless, the estimation suggests that no luminosity loss due to orbit jitter should be expected.

One of the major concerns is that ground motion could reduce the HL-LHC performance due to high beam losses at the primary collimators inducing frequent beam aborts. The risk of this strongly depends on the tail population, which is not well known. Small variations can have a large effect on the loss rate. Therefore, it is important to better study the tail population in order to improve the evaluation of the performance reduction from ground excitation and decide whether mitigation measures are necessary.

Declaration of competing interest

The authors declare that they have no known competing financial interests or personal relationships that could have appeared to influence the work reported in this paper.

Data availability

The authors are unable or have chosen not to specify which data has been used.

Acknowledgements

We would like to thank G. Baud, M. Gasior, J. Olexa, M. Soderen and D. Valuch for setting up the new data streams and interfaces to collect and log beam spectra with the ADT and DOROS BPMs of the LHC. Our gratitude goes to M. Fernandes Morais and Z. Arenas for providing details of the executed CE activities. Many thanks to D. Duarte Ramos for providing us with the simulations of the HL-LHC triplet transfer functions. We are as well grateful to B. Salvachua Ferrando for her advice on the LHC BLM threshold policy. This work was supported by the HL-LHC project and the STFC HL-LHC grant.

References

[1] V. Shiltsev, Review of observations of ground diffusion in space and in time and fractal model of ground motion, Phys. Rev. Spec. Top. Accel. Beams 13 (2010) 094801, http://dx.doi.org/10.1103/PhysRevSTAB.13.094801.

[2] L. Vos, Ground motion in LEP and LHC, Part. Accel. 50 (CERN-SL-94-69-BI, LHC-NOTE-299, CERN-LHC-Note-299) (1994) 221–231, 19 p.

[3] R. Steinhagen, S. Redaelli, J. Wenninger, Analysis of Ground Motion at SPS and LEP - Implications for the LHC, Tech. Rep. CERN-AB-2005-087, CERN, Geneva, Switzerland, 2005.

[4] J. Wenninger, N. Biancacci, L. Carver, P. Fessia, M. Gasior, M. Fitterer, M. Guinchard, J. Osborne, M. Poehler, Lessons learned from the civil engineering test drilling and earthquakes on LHC vibration tolerances, in: Proceedings of the LHC Performance Workshop, Chamonix, France, 2016, doi:https://indico.cern.ch/event/448109/.

[5] M. Cabon, C. Charrondiere, K. Develle, P. Fessia, M. Guichard, J. Wenningner, LHC Seismic Network Design, Installation and Operation, Tech. Rep. EDMS Report 1549343, CERN, Geneva, Switzerland, 2017.

[6] M. Guinchard, M. Cabon, C. Charrondière, K. Develle, P. Fessia, L. Lacny, J. Osborne, L. Scislo, J. Wenninger, Investigation and estimation of the LHC magnet vibrations induced by HL-LHC civil engineering activities, in: Proceedings of the 9th International Particle Accelerator Conference, Vancouver, BC Canada, 2018, WEPMF080, http://dx.doi.org/10.18429/JACoW-IPAC2018-WEPMF080.

[7] L. Rossi, O. Brüning, Progress with the high luminosity LHC project at CERN, in: Proccedings of the 10th International Particle Accelerator Conference, Melbourne, Australia, 2019, MOYPLM3, http://dx.doi.org/10.18429/JACoW-IPAC2019-MOYPLM3.

[8] Géothermies: développer et accompagner la géotermie à genève, 2023, https://www.geothermies.ch.

[9] S. Résonance Ingénieurs-Conseils, Déplacements Attendus Au CERN Lors de Séismes Induits, Tech. Rep. EDMS Report 1821506, CERN, Carouge, Geneva, Switzerland, 2016.

[10] M. Guinchard, L. Lancy, Vibration Effects of Future Civil Engineering Activities for Hilumi Project on the LHC Operation, Tech. Rep. EDMS Report 1487758, CERN, Geneva, Switzerland, 2016.

[11] M. Fitterer, G. Stancari, A. Valishev, R. Bruce, W. Höfle, M. Hostettler, P.S. Papadopoulou, G. Papotti, Y. Papaphilippou, D. Pellegrini, G. Trad, D. Valuch, G. Valentino, J. Wagner, X. Cai, MD1271: Effect of Low Frequency Noise on the Evolution of the Emittance and Halo Population, Tech. Rep. CERN-ACC-NOTE-2018-0006, CERN, Geneva, Switzerland, 2018.

[12] Y. Alexahin, On the emittance growth due to noise in hadron colliders and methods of its suppression, Nucl. Instrum. Methods Phys. Res. A 391 (1) (1997) 73–76, http://dx.doi.org/10.1016/S0168-9002(96)01190-4, Proceedings of the 11th International Advanced ICFA Beam Dynamic Workshop on Beam Cooling and Instability Damping.

[13] K. Ohmi, R. Calaga, W. Hofle, R. Tomas, F. Zimmermann, Beam-beam Effects With an External Noise in LHC, in: Proceedings of the Particle Accelerator Conference 2007 (PAC'07), JACoW Publishing, Geneva, Switzerland, 2007, pp. 1496–1498.

[14] W. Herr, B. Muratori, Concept of luminosity, in: CAS - CERN Accelerator School: Intermediate Accelerator Physics, no. CERN-2006-002, CERN, Geneva, Switzerland, 2006, p. 361.

[15] A. Gorzawski, K. Fuchsberger, M. Hostettler, T. Pieloni, J. Wenninger, Long-range beam-beam orbit effects in LHC, simulations and observations from machine operation in 2016, in: Proceedings of the 8th International Particle Accelerator Conference, JACoW Publishing, Copenhagen, Denmark, 2017, THPAB042, http://dx.doi.org/10.18429/JACoW-IPAC2017-THPAB042.

[16] S. Fartoukh, Achromatic telescopic squeezing scheme and application to the LHC and its luminosity upgrade, Phys. Rev. Spec. Top. Accel. Beams 16 (2013) 111002, http://dx.doi.org/10.1103/PhysRevSTAB.16.111002.

[17] J. Wenninger, Operation and Configuration of the LHC in Run 2, Tech. Rep. CERN-ACC-NOTE-2019-0007, CERN, Geneva, Switzwerland, 2019.

[18] E. Metral, S. Antipov, F. Antoniou, R. Appleby, G. Arduini, J. Barranco Garcia, P. Baudrenghien, N. Biancacci, C. Bracco, R. Bruce, X. Buffat, R. Calaga, L. Carver, E. Chapochnikova, M. Crouch, R. De Maria, S. Fartoukh, D. Gamba, M. Giovannozzi, P. Goncalves Jorge, W. Hofle, G. Iadarola, N. Karastathis, A. Lasheen, T. Mastoridis, L. Medina Medrano, A. Mereghetti, D. Mirarchi, B. Muratori, P. Papadopoulou, Y. Papaphilippou, D. Pellegrini, T. Pieloni, S. Redaelli, G. Rumolo, B. Salvant, M. Solfaroli Camillocci, C. Tambasco, R. Tomas Garcia, D. Valuch, Update of the HL-LHC Operational Scenarios for Proton Operation, Tech. Rep. CERN-ACC-NOTE-2018-0002, CERN, Geneva, Switzerland, 2018.

[19] R. De Maria, R. Bruce, D. Gamba, M. Giovannozzi, F. Plassard, High Luminosity LHC optics and layout HLLHCV1.4, J. Phys. Conf. Ser. 1350 (1) (2019) 012001, http://dx.doi.org/10.18429/JACoW-IPAC2019-MOPMP019.

[20] C. Collette, K. Artoos, M. Guinchard, C. Hauviller, Seismic response of linear accelerators, Phys. Rev. Spec. Top. Accel. Beams 13 (2010) 072801, http://dx.doi.org/10.1103/PhysRevSTAB.13.072801.

[21] D. Ziemiański, Ground Motion Measurements in Point 5, Tech. Rep. EDMS Report 1399820, CERN, Geneva, Switzerland, 2014.

[22] K. Schumann, M. Stipp, J.H. Behrmann, D. Klaeschen, D. Schulte-Kortnack, P and S wave velocity measurements of water-rich sediments from the Nankai trough, Japan, J. Geophys. Res.: Solid Earth 119 (2) (2014) 787–805, http://dx.doi.org/10.1002/2013JB010290.

[23] V.M. Juravlev, W. Coosemans, G. Ramseier, A. Seryi, A.I. Sleptsov, I.H. Wilson, Investigations of power and spatial correlation characteristics of seismic vibrations in the CERN LEP tunnel for linear collider studies, Tech. Rep. CERN-SL-93-53, CLIC-Note-217, CERN, Geneva, Switzerland, 1993.

[24] R. Bruce, R.W. Assmann, V. Boccone, C. Bracco, M. Brugger, M. Cauchi, F. Cerutti, D. Deboy, A. Ferrari, L. Lari, A. Marsili, A. Mereghetti, D. Mirarchi, E. Quaranta, S. Redaelli, G. Robert-Demolaize, A. Rossi, B. Salvachua, E. Skordis, C. Tambasco, G. Valentino, T. Weiler, V. Vlachoudis, D. Wollmann, Simulations and measurements of beam loss patterns at the CERN Large Hadron Collider, Phys. Rev. Spec. Top. Accel. Beams 17 (2014) 081004, http://dx.doi.org/10.1103/PhysRevSTAB.17.081004.

[25] R. Assmann, Collimators and beam absorbers for cleaning and machine protection, in: Proceedings of the 2nd LHC Project Workshop (Chamonix XIV), CERN, Geneva, Switzerland, 2005, pp. 261–267, doi:https://cds.cern.ch/record/987838.

[26] C. Charrondiere, M. Cabon, K. Develle, M. Guinchard, Ground vibration monitoring at CERN as part of the international seismic network, in: Proceedings of the 16th International Conference on Accelerator and Large Experimental Physics Control Systems, Barcelona, Spain, 2017, THPHA134, http://dx.doi.org/10.18429/JACoW-ICALEPCS2017-THPHA134.

[27] Swiss seismological service (SED), 2023, http://www.seismo.ethz.ch.

[28] D. Ramos, M. Oliver, M. Moretti, Response of the HL-LHC triplet cryostat to base excitation induced vibrations: status and plans, in: Proceedings of the 8th HL-LHC Collaboration Meeting, CERN, Geneva, Switzerland, 2018.

[29] V. Zhabitsky, W. Höfle, G. Kotzian, E. Montesinos, M. Schokker, D. Valuch, Beam tests of the LHC transverse feedback system, in: Proceedings of the 22th Russian Particle Accelerator Conference, Protvino, Russia, 2010, THCHX01.

[30] M. Ojeda Sandonis, P. Baudrenghien, A. Butterworth, J. Galindo, W. Höfle, T. Levens, J. Molendijk, F. Vaga, D. Valuch, Processing high-bandwidth bunch-by-bunch observation data from the RF and transverse damper systems of the LHC, in: Proceedings of the 15th International Conference on Accelerator and Large Experimental Physics Control Systems, Melbourne, Australia, 2015, WEPGF062, http://dx.doi.org/10.18429/JACoW-ICALEPCS2015-WEPGF062.

[31] J. Olexa, Design and Optimization of the Beam Orbit and Oscillation Measurement System for the Large Hadron Collider (Ph.D. Thesis), Slovak Tech. U., Bratislava, Slovakia, 2018, CERN-THESIS-2018-185.

[32] J. Pistrol, F. Kopf, D. Adam, S. Villwock, W. Völkel, Ambient vibration of oscillating and vibrating rollers, in: Proceedings of the Vienna Congress on Recent Advances in Earthquake Engineering and Structural Dynamics, Vienna, Austria, 2013, p. 167.

[33] J. Wagner, R. Bruce, H. Garcia Morales, W. Höfle, G. Kotzian, R. Kwee-Hinzmann, A. Langner, A. Mereghetti, E. Quaranta, S. Redaelli, A. Rossi, B. Salvachua Ferrando, R. Tomas Garcia, D. Valuch, G. Valentino, G. Stancari, Active Halo Control Through Narrow-Band Excitation with the ADT, Tech. Rep. CERN-ACC-NOTE-2016-0009, CERN, Geneva, Switzerland, 2016.

[34] P. Racano, Beam Profile Reconstruction of the LHC Beams Using Collimator Scans (Master Thesis), Sapienza - Università di Roma, Italy, 2019, CERN–THESIS–2019–429.

[35] O. Aberle, I. Béjar Alonso, O. Brüning, P. Fessia, L. Rossi, L. Tavian, M. Zerlauth (Eds.), High-Luminosity Large Hadron Collider (HL-LHC): Technical Design Report, in: CERN Yellow Reports: Monographs, no. CERN-2020-010, CERN, Geneva, Switzerland, 2020, http://dx.doi.org/10.23731/CYRM-2020-0010.

[36] A. Mereghetti, R. Bruce, E. Holzer, M. Kalliokoski, S. Redaelli, B. Salvachua Ferrando, BLM thresholds and damage limits for collimators, in: 6th Evian Workshop on LHC Beam Operation, no. CERN-ACC-2015-376, Evian, France, 2015, p. 197.

[37] B. Lindstrom, P. Bélanger, L. Bortot, R. Denz, M. Mentink, E. Ravaioli, F. Mateos, R. Schmidt, J. Uythoven, M. Valette, A. Verweij, C. Wiesner, D. Wollmann, M. Zerlauth, Fast failures in the LHC and the future high luminosity LHC, Phys. Rev. Accel. Beams 23 (2020) 081001, http://dx.doi.org/10.1103/PhysRevAccelBeams.23.081001.

[38] D. Gamba, R. Corsini, M. Guinchard, M. Schaumann, J. Wenninger, Estimated impact of ground motion on HL-LHC beam orbit, in: Proceedings of the 9th International Particle Accelerator Conference, Vancouver, BC Canada, 2018, THPAF040, http://dx.doi.org/10.18429/JACoW-IPAC2018-THPAF040.

[39] A. Verdier, L. Vos, Ground Motion Model for the LHC, Tech. Rep. CERN-LHC-Project-Report-444, CERN, Geneva, Switzerland, 2000.